18th Australasian Fluid Mechanics Conference
Launceston, Australia
3-7 December 2012

Volumetric Measurements by Tomographic PIV of an Open Channel Flow Behind a Turbulent Grid

T. Earl[1], R. Ben Salah[2], L. Thomas[2], B. Tremblais[3], S. Cochard[1], L. David[2]

[1]School of Civil Engineering
University of Sydney, NSW 2006, Australia

[2]Institut Pprime
Université de Poitiers, 86968 Futuroscope, France

[3]Départment XLIM-SIC
Université de Poitiers, 86968 Futuroscope, France

Abstract

This paper investigates the energy dissipation rate behind two combinations of trash racks (or meshes) in an open channel flow from tomo-PIV measurements. Five trash rack assemblies divided the flume into four identical pools. Each trash rack assembly is composed of a fine wire mesh and two regular square grids, characterised by their mesh size M. The Reynolds numbers with respect to M were 4300 and 9600 corresponding to a mean velocity U through each pool between 0.35 and 0.315 m/s. This aim of this paper is to investigate the turbulent energy dissipation behind two configurations of regular grids in an open channel.

Introduction

The measurement of turbulence in a flow generated behind a regular grid has been extensively investigated, with origins linked to the conception of the hot-wire anemometer and used in Taylor's Statistical Theory of Turbulence (1935). The regular grid was designed to generate homogeneous isotropic turbulence (HIT). A number of different time-resolved, point measurement techniques are used to measure small scale characteristics of turbulence and the mean turbulent energy dissipation rate $\langle\varepsilon\rangle$, such as hot wire anemometry (HWA), laser Doppler velocimetry (LDV) and other novel probes [1]. However, these techniques are limited in that they cannot resolve large vortex structures.

With the advent of particle image velocimetry (PIV), planar, spatially resolved measurements of turbulence have been made [4, 7]. From these results, it has been possible to measure the anisotropy of these turbulent flows by measuring two components of velocity. Stereo PIV can recover the 3 velocity components but not the full velocity gradient tensor. Only the velocity gradients that lie in the measurement plane can be computed, as the measurement takes place in a 'thin' planar light sheet. Therefore, these techniques make the assumption about the isotropy of the flow if one were to calculate the instantaneous velocity tensors to obtain energy dissipation.

With techniques such as tomo-PIV [5], it is possible to obtain volumetric velocity fields, i.e. all 9 components of the velocity gradient tensors. Tomo-PIV is technique that allows the determination of three component, three dimensional (3C-3D) velocity fields [5, 2, 8]. The basic principal is to record, with typically four cameras, two sets of simultaneous images of particles that are seeded in the flow and illuminated by a thick laser sheet over a small time step. Those images are then used to reconstruct the light density distribution of each volume. Velocity vector fields are then obtained by performing a correlation between the two volumes, which deduces the most probable displacements of groups of particles. Akin to 2D PIV techniques, there are spatial limitations due to the interrogation window size of PIV measurements [6, 7]. Recently Worth *et al.* [12] and Buchmann *et al.* [3] used tomographic PIV to measure turbulence, the later paper dealing specifically with grid generated turbulence in water.

This paper details the experimental facility and initial results obtained from measurements behind two configurations of regular grids in an open channel. The aim is to investigate the flow structures and turbulence dissipation of the flow.

Experimental Details

Experiments were conducted in an open channel (figure 1) at Institut Pprime at the Universitè de Poitiers, France. The inclined channel was rectangular in cross section with dimension 500×304 mm^2 (height $\times$ width, W) and had 30 mm thick perspex walls and base to allow full optical access. The channel was divided into 4 identical pools that were separated by trash rack assemblies, described further in *Trash Rack and Grid Details*. The inclination of the channel for the two trash rack assembly types presented was 5%. The weir gate height was adjusted so that there was a regular head loss, ΔH, across each trash rack with a constant flow rate of $Q = 34$ L/s.

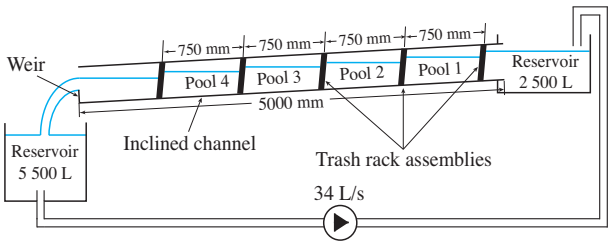

Figure 1: Schematic of experimental set-up.

Trash Rack and Grid Details

Each pool was separated by a trash rack assembly that was approximately vertical in orientation. The trash racks were comprised of, from upstream to downstream, a fine wire mesh and then a pair of regular grids that were fabricated from 2 mm thick stainless steel plates. The grid pairs used were G1-G2 and G3-G4, with square opening geometries as shown in figure 2. There was a stream-wise spacing between the components of the trash rack that was nominally 90 mm. The solidity ratios σ, defined by $\sigma = (D/M)(2 - D/M)$ are also defined in figure 2, where D is the thickness of each bar and M is the centre-to-centre bar spacing of the grid. The grid geometries furthermost downstream,

that is G2 and G4, are used for the dimensionless analysis in this paper as the resulting turbulence downstream is characterised by these grids.

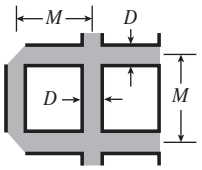

GRADES (mm)

	M	D	σ
Mesh	2.4	0.4	0.31
G1	12	2	0.31
G2	14	4	0.49
G3	30	5	0.31
G4	35	10	0.49

Figure 2: Grid geometries.

Flow properties

The water temperature was 15.4±0.5° C, with associated kinematic viscosity $\nu \approx 1.15 \times 10^{-6}$ m^2/s . The mean velocity of the flow through each pool, $U = Q/(h_c W)$, where h_c is the flow depth at the centre of the pool, was approximately 0.35 m/s and 0.315 m/s for the G1-G2 and G3-G4 configurations respectively. Likewise, the respective Reynolds numbers with respect to grid geometry were 4300 and 9600. The hydraulic radius, $R_h = h_c W/(2h_c + W)$ for this channel was in the order of 0.1 m for both combinations.

Tomo-PIV Details

Tomo-PIV measurements were taken in pool 3 to ensure a developed flow (figure 3). The tomo-PIV system was comprised of four 1600 × 1200 px^2 8 bit cameras positioned symmetrically in an inverted pyramid configuration, with nominal declination and inward angles of approximately 20° (see figure 3). All cameras were fitted with 50 mm lenses, 532 nm pass optical filters and lens mounted Scheimpflug adapters, adjusted so that the camera focal planes were coincident with the laser sheet. Additionally, the apertures were set at at $f_\# = 22$ during acquisition for superior depth of focus. Neutrally buoyant, spherical polyamide particles of mean diameter $d_{50} \approx 56$ μm were used to seed the flow.

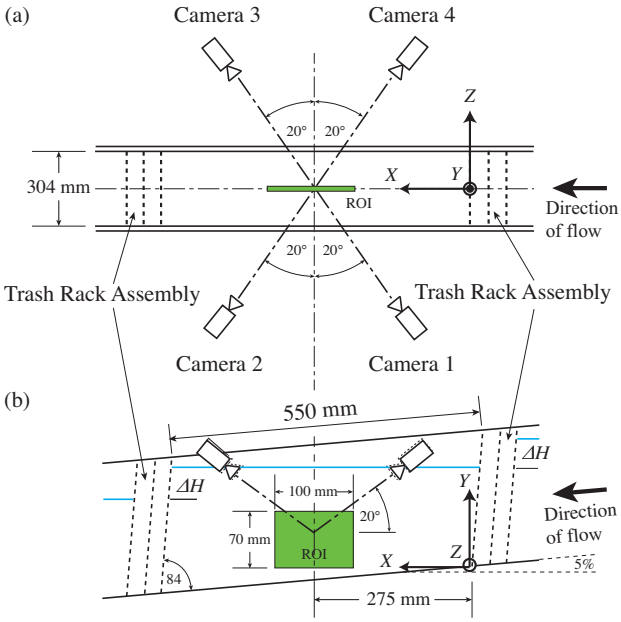

Figure 3: Schematic of Pool 3 showing measurement volume or region of interest (ROI) in (a) plan and (b) elevation. The origin and axis orientation along with inverted pyramid configuration of the cameras are shown.

A thick laser sheet was used to illuminate the measurement volume, realised with a Twins CFR ND:YAG laser with 120 mJ per pulse. The measurement volume was 100 × 70 × 15 mm^3 ($X \times Y \times Z$) and was positioned centrally and aligned with the flow direction in pool 3. This positioning corresponds to a dimensionless region $16 \leq x/M \leq 23$ for the G1-G2 configuration and $6.4 \leq x/M \leq 9.3$ and for the G3-G4 configuration downstream.

The time between corresponding images, Δt, was 2 ms, chosen to achieve mean particle displacements of 10 px for each camera. These image pairs (which make a velocity field) were acquired at 5 Hz. The total data set consists of 5000 images per camera, corresponding to 2500 velocity fields for each grid configuration. The initial results presented in this article correspond to approximately 250 velocity fields for each configuration.

The tomo-PIV software used was developed using the SLIP library [10] and developed at the Université de Poitiers. Reconstruction was performed with MinLOS–MART (minimum line-of-sight, multiplicative algebraic reconstruction technique) [9]. The volume size was 1380 × 920 × 211 voxels^3 with each cubic voxel having sides of 0.076 mm, approximately 15% larger than the pixel size. Processing was undertaken on an Intel Core i7 2.93 GHz machine, and each 2 GB volume took in the order of 40 minutes to reconstruct.

Treatment of data

The tomo-PIV process is sensitive to a number of parameters, so image processing and calibration methods must be carefully considered. Image processing to remove background noise was conducted with a sliding 16 × 16 px^2 mean window to ensure a homogeneous particle per pixel of $ppp \approx 0.022$ for all cameras at both time-steps. A gaussian filtering kernel was then applied to smooth particle images, the kernel size chosen to match the average particle diameter. Small bubble entrainment in the water due to the free surface and subsequent turbulent mixing through the trash rack assembly was evident, and as these created 'particles' larger than the mean, detracted from the quality of image reconstruction. A pinhole model was used to calibrate the cameras. A calibration plate was traversed at 3±0.005 mm spacing through the illuminated volume. Due to the large deviations in the lines-of-sight of each camera through the thick perspex walls, the camera calibration was improved with a self calibration technique analogous to Wieneke [11].

Preliminary results are obtained with a single pass cross-correlation program. A 64 × 64 × 64 voxel^3 correlation volume with 50% overlap was used to find the most probable displacement of particles across the two reconstructed volumes. This resulted in 6000 vectors per acquisition at a spatial resolution of 4.9 × 4.9 × 4.9 mm^3. A 5 × 5 × 5 filter kernel was used that replaced spurious vectors with the median vector in the filtering kernel. As tomographic reconstruction has been shown to be particularly susceptible to noise [12], a bilateral filter was used to filter the velocity fields, which was preferred over a gaussian filter as it preserves edges.

Results

The data sets have been set to dimensionless volumes downstream by dividing through by the respective M for each configuration. This is shown to be appropriate after comparing the energy dissipation rate $\langle \varepsilon \rangle$ as a function of X for both cases (figure 8), where $\langle \ldots \rangle$ denotes ensemble averaging.

The tomo-PIV captured the global flow characteristics. Figure 4 shows contour plots in the XY-plane of u for the G3-G4 configuration that were averaged over 250 velocity fields over the

laser sheet thickness ΔZ. The measured average u velocity of 0.324 m/s correlates well with $\bar{U}$ estimated from the flow rate. Similarly, the time averaged results for the G1-G2 plots yield a similar figure, albeit with a measured average $\underline{u}$ of 0.354 m/s, which also corresponds well with the expected $\bar{U}$. The contours indicate that the flow is decelerating in the stream-wise direction; this is explained by the expansion of the volume of flow. There is a declination of the channel base in the stream wise direction however there is a comparatively level free surface. The contour plot also indicates that more velocity fields are required to form the mean field, owing to the high level of variability.

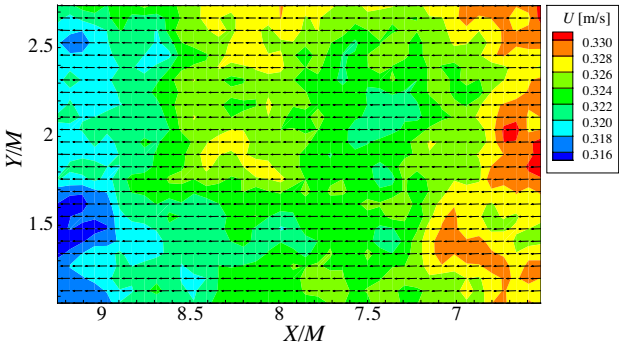

Figure 4: Mean velocity vector field showing contours of u (m/s) and velocity vectors u and v indicating flow from right to left (in positive X-direction, for configuration G3-G4.

The instantaneous vorticity fields ω were analysed to compare the level of vorticity present in each configuration. The tomo-PIV allows for full recovery of the velocity gradient tensors and hence vorticity. From figure 5, vorticity iso-surfces showing ω_z are plotted: The presence and power of vortex structures is greater in the G3-G4 case. It is noted that G3-G4 has larger grid sizes in the trash rack and in a dimensionless sense, it is nearer to the back of the trash rack. In the following section it is shown that these results give good qualitative agreement to the decay dissipated energy of the system, as with the decay in energy it is expected that the level of vorticity decays also.

Local Dissipation Rate

The trace of the local dissipation tensor, with components ε_{ij}

$$\varepsilon_{ij} = 2\nu \sum_k \frac{\partial u_i}{\partial X_k} \frac{\partial u_j}{\partial X_k} \tag{1}$$

is used to calculate the local dissipation rate $\langle \varepsilon \rangle$ in the flow.

The average dissipation of the flow does not evolve over time, as observed in figure 6. It was found that the dissipation is approximately 3.4 times greater in the G3-G4 configuration than in the G1-G2 configuration. The turbulent kinetic energy is greater in the G3-G4 configuration and is dissipated in the basin (figure 5).

The time averages were considered to determine whether the statistics are well converged. The convergence of the mean dissipation rate is presented in figure 7. It is observed that convergence is achieved after 200 velocity fields.

Finally, the evolution in the spatial direction of the flow, the dissipation of space-time average, is presented in figure 8. In this figure, the data are averaged over time and in the planes perpendicular to the flow. It can be seen that the magnitude of dissipation decreases exponentially, with a coefficient of attenuation of 0.106. Initial studies into the eigenvalues of the energy tensor dissipation were undertaken (not presented here).

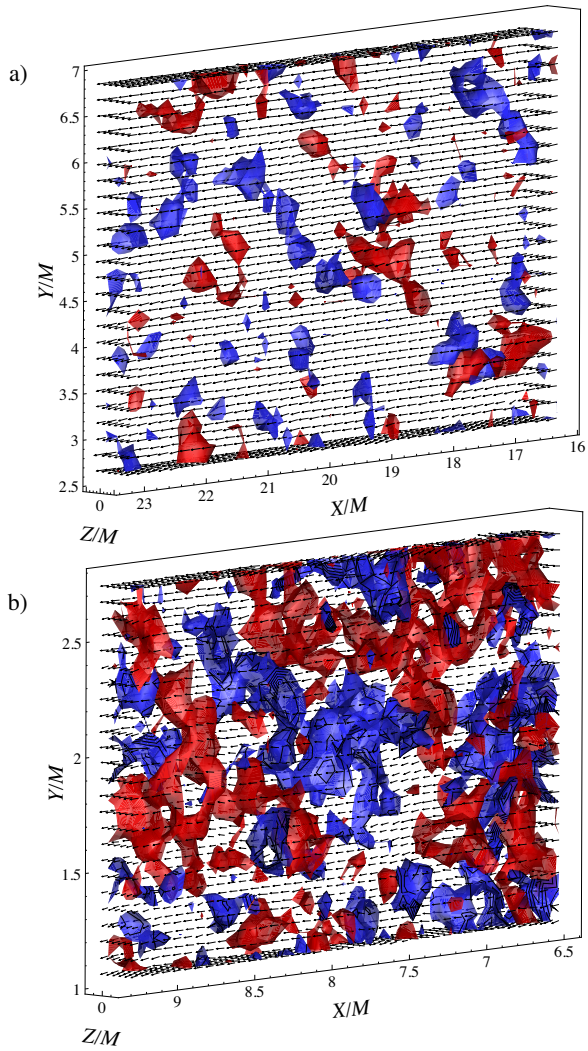

Figure 5: ω_z iso-contours at 0.008 m^{-2} (red) and -0.008 m^{-2} (blue) for configuration (a) G1-G2 and (b) G3-G4 with velocity vectors.

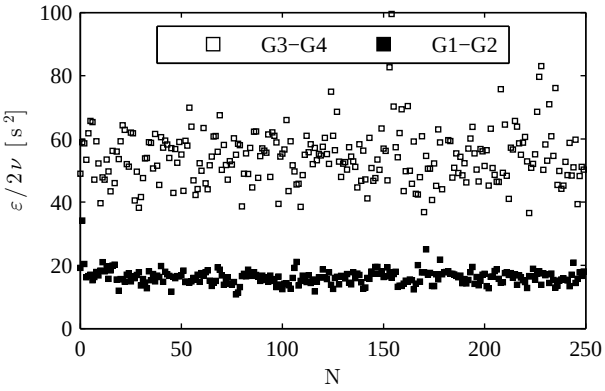

Figure 6: Evolution of the temporal average of the dissipation in G1-G2 and G3-G4, where N indicates the number of velocity fields considered.

It was found that they evolve in the parallel (when considering the spatial direction of the flow, following figure 8), indicating anisotropy of the dissipation. These results are still being analysed as this paper goes to press, but the initial findings show the

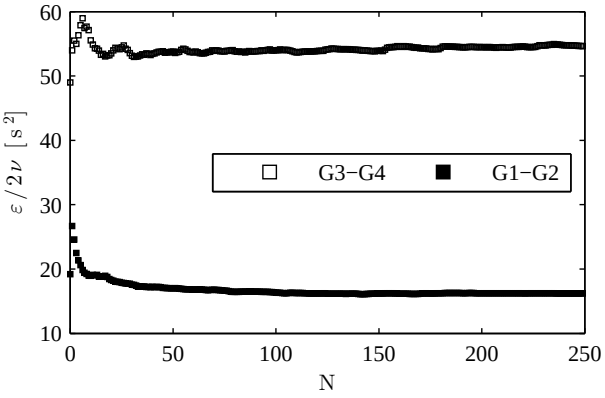

Figure 7: Evolution of the mean dissipation over time for G1-G2 and G3-G4, where N indicates the number of velocity fields considered.

benefits of recovering all velocity gradient tensors when studying turbulence, using a technique such as tomo-PIV.

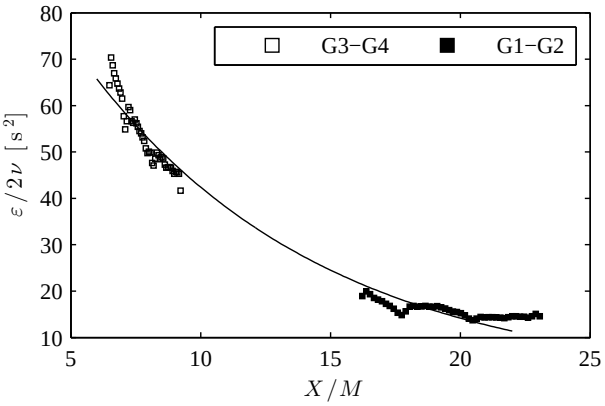

Figure 8: Energy dissipation in the direction of flow for both G1-G2 and G3-G4 configurations with power law fit.

Conclusions

Tomo-PIV was used to measure the flow in a pool of an inclined open channel behind a trash rack. Two assembly configurations of grids were compared: analysis of the vorticity and energy dissipation show qualitative and quantitative agreement of the decay of turbulent kinetic energy following a power law. The energy dissipation was found to decay exponentially in the direction of flow. By normalising with mesh size, the same power law could be used to describe the decay. Initial analyses of the eigenvalues of the energy dissipation tensors show anisotropy of the decay, a finding made possible by the recovery of the full velocity gradient tensors through tomo-PIV.

Future Work

Two trash rack configurations that form part of the experimental data set were not included herein. More data are being analysed to ensure the quality of the statistical analysis. Furthermore, analysis of the relevant length scales is required to describe the evolution of dissipation.

Acknowledgements

The authors would like to express gratitude for the continued support of an Australian Postgraduate Award (APA) and Joan McConnell scholarship. The experiments were conducted at the Université de Poitiers, France, and were funded by l'ANR VIVE3D and FEDER.

References

[1] R. A. Antonia, P. Lavoie, L. Djenidi, and A Benaissa. Effect of a small axisymmetric contraction on grid turbulence. *Experiments in Fluids*, 49(1):3–10, July 2009.

[2] C. Atkinson and J. Soria. An efficient simultaneous reconstruction technique for tomographic particle image velocimetry. *Experiments in Fluids*, 47(4-5):553–568, August 2009.

[3] N A Buchmann, C Atkinson, and J Soria. Tomographic and Stereoscopic PIV measurements of Grid- generated Homogeneous Turbulence. In *15th Int Symp on Applications of Laser Techniques to Fluid Mechanics Lisbon, Portugal, 05-08 July, 2010*, 2010.

[4] J. I. Cardesa, T. B. Nickels, and J. R. Dawson. 2D PIV measurements in the near field of grid turbulence using stitched fields from multiple cameras. *Experiments in Fluids*, 52(6):1611–1627, February 2012.

[5] G. E. Elsinga, F. Scarano, B. Wieneke, and B. W. Oudheusden. Tomographic particle image velocimetry. *Experiments in Fluids*, 41(6):933–947, October 2006.

[6] J M Foucaut, J Carlier, and M Stanislas. PIV optimization for the study of turbulent flow using spectral analysis. *Measurement Science and Technology*, 15(6):1046–1058, June 2004.

[7] P. Lavoie, G. Avallone, F. Gregorio, G. P. Romano, and R. A. Antonia. Spatial resolution of PIV for the measurement of turbulence. *Experiments in Fluids*, 43(1):39–51, May 2007.

[8] M. Novara, K. J. Batenburg, and F. Scarano. Motion tracking-enhanced MART for tomographic PIV. *Measurement Science and Technology*, 21(3):1–18, March 2010.

[9] T Putze and H-G Maas. 3D Determination of very dense particle velocity fields by tomographic Reconstruction from four camera views and voxel space tracking. *The International Archives of the Photogrammetry, Remote Sensing and Spatial Information Sciences*, XXXVII:33–38, 2008.

[10] B Tremblais, L David, D Arrivault, J Dombre, L Chatellier, and L Thomas. SLIP: Simple Library for Image Processing (version 1.0), http://www.sic.sp2mi.univ-poitiers.fr/slip/, 2010.

[11] B Wieneke. Volume self-calibration for 3D particle image velocimetry. *Experiments in Fluids*, 45:549–556, 2008.

[12] N. A. Worth, T. B. Nickels, and N. Swaminathan. A tomographic PIV resolution study based on homogeneous isotropic turbulence DNS data. *Experiments in Fluids*, 49(3):637–656, February 2010.